

Paddy Rice Experiment in the Sanjiang Plain (PRESP 2019)

Field Measurement Report

Version 1.0

Hongliang Fang, Yinghui Zhang, Yao Wang, Sijia Li

State Key Laboratory of Resources and Environmental Information System,
Institute of Geographic Sciences and Natural Resources Research,
Chinese Academy of Sciences

March 2020



Participants

Prof. Hongliang Fang
Principle Investigator
LREIS, Institute of Geographic Sciences and Natural Resources Research
Chinese Academy of Sciences
Beijing 100101, China
Email: fanghl@lreis.ac.cn

Yinghui Zhang, Yao Wang, Sijia Li
PhD. students
LREIS, Institute of Geographic Sciences and Natural Resources Research
Chinese Academy of Sciences
Beijing 100101, China

Acknowledgments

The field campaign was supported by the National Key Research and Development Program of China [2016YFA0600201]. We would like to thank the Sanjiang Experimental Station of Wetland Ecology, Chinese Academy of Sciences for the help with our fieldwork. We also thank the farmers for allowing us to make use of their fields for in situ measurements.

Revision History

<i>Revision Date</i>	<i>Changes</i>	<i>Major contributor</i>
2020-1-20	Initial draft	Yinghui Zhang

Table of Contents

1. Overview	1
2. Site description and ground sampling	2
2.1 Site description.....	2
2.2 Sampling strategy.....	2
3. Field measurement methods	5
3.1 LAI-2200.....	5
3.2 DHP.....	7
3.3 AccuPAR.....	10
3.4 AvaField	11
4. Results	13
4.1 Effective PAI.....	13
4.2 FAPAR	14
4.3 Gap fraction.....	15
4.4 Clumping index.....	16
4.5 fCover.....	17
4.6 ALA	18
4.7 Spectral reflectance curve	19
5. Quality assurance	21
6. Data access and citation	22
6.1 Data access	22
6.2 Citation.....	22
References	23

List of Figures

Fig. 1. The left panel shows the distribution of five plots on Google earth images. The right upper panel shows a photo taken in a paddy rice field. The right low panel shows the sampling strategy within an ESU for LAI-2200(black dot), AccuPAR (Black dot), DHP (red line) and AvaField (green dot).	3
Fig. 2. Sample photos for the main growing stages: (a) tillering stage (Jun 23 and July 1, 2019); (b) jointing stage (Jul 10 and Jul 16, 2019); (c)flowering stage (Jul 29, and Aug 12, 2019); (d) maturing stage (Aug 18 and Aug 25, 2019).....	4
Fig. 3. LAI-2200 with a single sensor and the sampling strategy for LAI-2200 over paddy rice field	5
Fig. 4. LAI-2200 field measurement (left: above the canopy; right: below the canopy) ...	5
Fig. 5. Nikon D5100 equipped with Sigma F2.8 EX DC circular fisheye. An ultraviolet cap was used to prevent dust or rain from the lens.	7
Fig. 6. The downward DHP images obtained during different main growing stages corresponding to Fig. 2: (a) tillering stage (Jun 23 and July 1, 2019); (b) jointing stage (Jul 10 and Jul 16, 2019); (c)flowering stage (Jul 29, and Aug 12, 2019); (d) maturing stage (Aug 18 and Aug 25, 2019).	8
Fig. 7. An example of photo classification in the CAN_EYE software. Green indicates the rice and soil is the background. The operators have been masked.	9
Fig. 8. AccuPAR model LP-80 PAR/LAI ceptometer	10
Fig. 9. AccuPAR field measurement.....	11
Fig. 10. AvaField-3 portable field spectroradiometer	11
Fig. 11. AvaField field measurement	12
Fig. 12. Seasonal variation of the effective PAI (PAI _{eff}) estimated from LAI-2200, DHP, for the five plots. Panels (a)–(e) for plots A–E and panel (f) the average of all plots.	14
Fig. 13. Seasonal variations of the FAPAR in the morning (10:30 am, FAPAR _{am}) and afternoon (18:00 pm, FAPAR _{pm}) estimated from AccuPAR and diffuse FAPAR (FAPAR _{dif}), direct FAPAR (FAPAR _{dir}) from DHP for the five plots. Panels (a)–(e) for plots A–E and panel (f) the average of all plots.....	15
Fig. 14. Seasonal variations of the gap fraction at different view zenith angles from LAI-2200 and DHP. For DHP, the measured effective gap fractions from CAN_EYE V6.1 are shown. The Panel of the last column shows the average gap fractions from LAI-2200 and DHP and the transmittance from AccuPAR at about 10:30 am.....	16
Fig. 15. Seasonal variation of the clumping indices (CI) at different view zenith angles from LAI-2200 and DHP. The Panel of the last column shows the overall CI from LAI-2200 and DHP.	17
Fig. 16. Seasonal variations of fCover calculated from LAI-2200 and DHP.....	18
Fig. 17. Seasonal variation of ALA calculated from LAI-2200 and DHP. Solid and dashed lines represent effective and true ALAs retrieved from DHP, respectively.	19
Fig. 18. Spectral reflectance curve (400 nm–1000 nm) measured over the season.	20

List of Tables

Table 1. Structural and optical variables derived from field measurements.	1
Table 2. Information for the five plots in the study area.	3
Table 3. The weighting factors of each ring for LAI-2200.	6
Table 4 Data details at five plots	13
Table 5. Field measurement log.....	24

List of Acronyms and Abbreviations

ACFs	Apparent clumping factors
ALA	Average leaf angle
CI	Clumping index
DHP	Digital hemispherical photography
DOY	Day of year
ESU	Elementary sampling unit
FAPAR	Fraction of absorbed photosynthetically active radiation
FAPAR _{am}	FAPAR measured in the morning at about 10:30 am
FAPAR _{pm}	FAPAR measured in the afternoon at about 18:00 pm
FAPAR _{dir}	Direct FAPAR
FAPAR _{dif}	Diffuse FAPAR
fCover	Fraction of vegetation cover
LAI	Leaf area index
LAD	Leaf angle distribution
LUT	Look up table
NIR	Near-infrared band
PAI	Plant area index
PAI _{eff}	Effective plant area index
PAR	Photosynthetically active radiation
SAI	Stem and seeds area index
SZA	Solar zenith angle
VALERI	Validation of Land European Remote Sensing Instruments
VIS	Visible band

1. Overview

The Paddy Rice Experiment in the Sanjiang Plain (PRES-P) was conducted at the paddy rice fields in Honghe Farm, NE China (47°39.11' N, 133°31.31' E), from the end of June to the end of August in 2019. The objective of the field campaign is to collect consistent ground FAPAR and LAI data for paddy rice in order to support the validation of FAPAR and LAI products obtained by remotely sensed data. The site is about 3 km × 3 km with five plots scattered in four corners and the center. Several optical instruments, including LAI-2200, Digital Hemispherical Photography (DHP), AccuPAR, and AvaField were used to obtain LAI and other structural and optical parameters (Table 1).

Table 1. Structural and optical variables derived from field measurements.

	LAI-2200	DHP	AccuPAR	AvaField
PAI		√		
PAI _{eff}	√	√		
Angular gap fraction	√	√		
Integrated gap fraction	√	√	√	
Angular ACF/CI	√	√		
Integrated ACF/CI	√	√		
ALA	√	√		
fCover	√	√		
FAPAR		√	√	
Reflectance				√

2. Site description and ground sampling

2.1 Site description

The study area is located at the Honghe Farm in the Heilongjiang Province, NE China. The site experiences a typical humid continental monsoon climate, with long cold winter and warm and humid summer. The mean annual temperature is 2.52°, with monthly mean temperature ranging from -20° in January to about 22° in July. The average annual precipitation is approximately 558 mm, with substantial interannual and seasonal variation (Song et al., 2009). The mean altitude of this site is approximately 56 m. The main soil types are the albic bleached meadow soils (Albaqualfs) (Yang et al., 2013). The water and soil in these marshes are completely frozen from late October to April and begin to thaw in late April.

This site was originally a wetland and has been converted to plant paddy rice since 1997. The paddy rice fields are flat with more than 5 km homogeneity and large rectangular fields approximately 30 m × 100 m in size. A single rice variety (Japonica) is grown in this region. The rice-cropping practices are uniform, growing once a year during the summer season (May to September), with a maturation stage for about 120-150 days. The dates for the panicle formation stage, heading stage, and maturity stage are mid-June, mid-July, and early August, respectively. Paddy fields are irrigated with ground water throughout the season. The soil surface is under flooded conditions with a depth of about 5-12 cm during most of the growing periods except the time when the water is emptied for medicinal purposes because of weeds or pests.

2.2 Sampling strategy

Five plots (A, B, C, D, and E), four at the four corners and one at the center, were chosen for intensive ground-based measurements (Fig. 1). Each plot was planted with a cultivar type and managed individually. Within each plot, 4 Elementary Sampling Units (ESUs), in the size of 10×10 m² or 15×15 m² were selected. ESUs were located at least 1.5 m away from the field borders. The main information of the five plots are showed in Table 2.

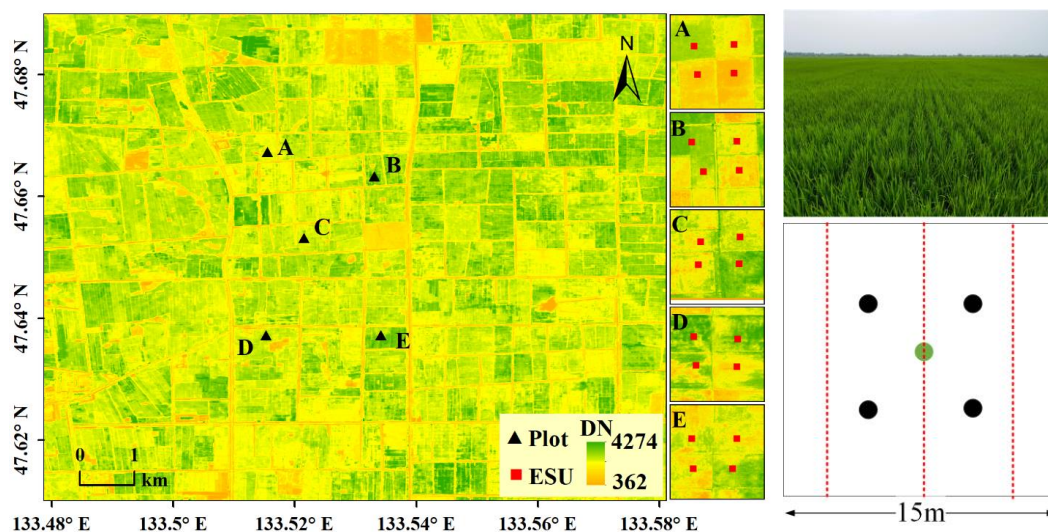


Fig. 1. The left panel shows the distribution of five plots on Google earth images. The right upper panel shows a photo taken in a paddy rice field. The right low panel shows the sampling strategy within an ESU for LAI-2200(black dot), AccuPAR (Black dot), DHP (red line) and AvaField (green dot).

Table 2. Information for the five plots in the study area.

Plot ID	Center location	ESU size(m)	Notes
A	133.515°E, 47.667°N	15×15	
B	133.532°E, 47.663°N	10×10	Some weeds exited after 12 July
C	133.523°E, 47.653°N	10×10	
D	133.515°E, 47.637°N	15×15	
E	133.534°E, 47.637°N	15×15	

Ground LAI measurement was conducted from June 22, shortly after the rice transplantation, to August 26 when the rice is maturing. Fig. 2 shows some photos taken at the main growing stages in the study area. Field measurements were performed sequentially for the five plots every week, in order to capture the canopy structural dynamics. AccuPAR and AvaField measurements were conducted at 10:00 - 10:30 am. AccuPAR, LAI2200 and DHP measurements were conducted near sunset or under overcast conditions as the sensitivity of the parameters and the retrieval errors increase under direct illuminations (Fang et al., 2018, 2014).

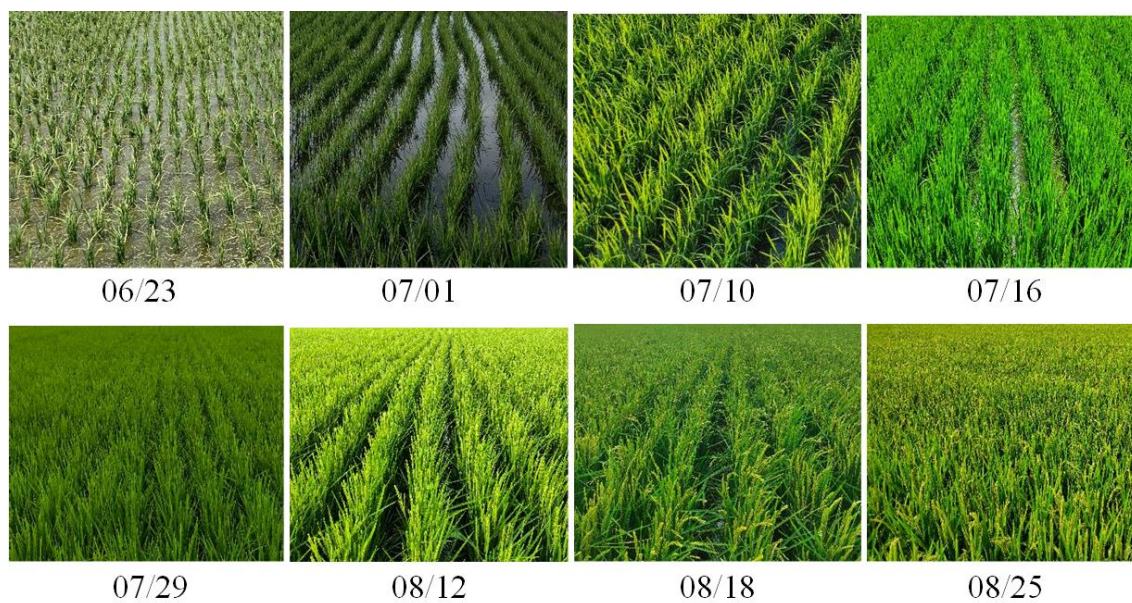


Fig. 2. Sample photos for the main growing stages: (a) tillering stage (Jun 23 and July 1, 2019); (b) jointing stage (Jul 10 and Jul 16, 2019); (c) flowering stage (Jul 29, and Aug 12, 2019); (d) maturing stage (Aug 18 and Aug 25, 2019).

3. Field measurement methods

3.1 LAI-2200

A LAI-2200 Plant Canopy Analyzer (PCA) (LI-COR Inc., Lincoln, Nebraska) was used to estimate the rice PAI as all parts of the plants, including green leaves, yellow leaves, stems, and seeds contribute to the canopy transmittance process (Fig. 4). All measurements were conducted under diffuse conditions. Following the instruction manual for row crops, ground measurements were made along diagonal transects between the rows (Fig. 5). Two repeats were made for each measurement with one above and four below canopy readings (Fig. 6). For below canopy measurements, the instrument was held about 5 cm above the background soil or shallow water. Throughout the season, a 270° view cap was used to shield the sensor from the operator. All values from four measurements were averaged to obtain the values at the ESU level.

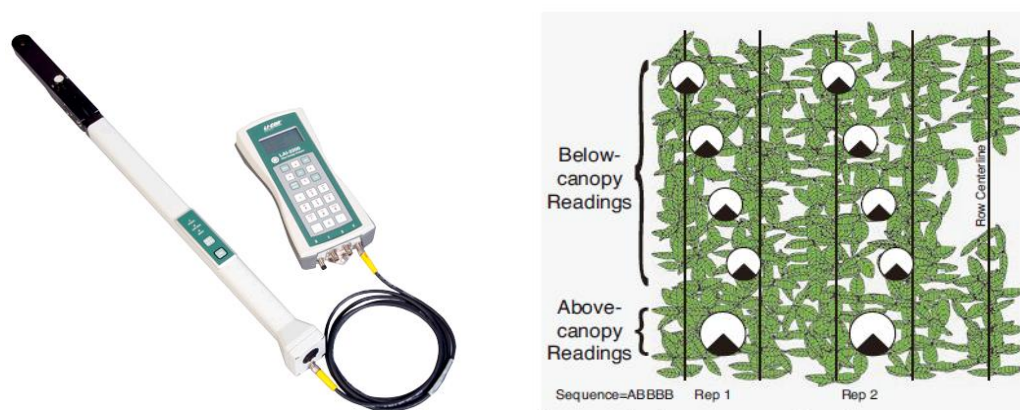


Fig. 3. LAI-2200 with a single sensor and the sampling strategy for LAI-2200 over paddy rice field

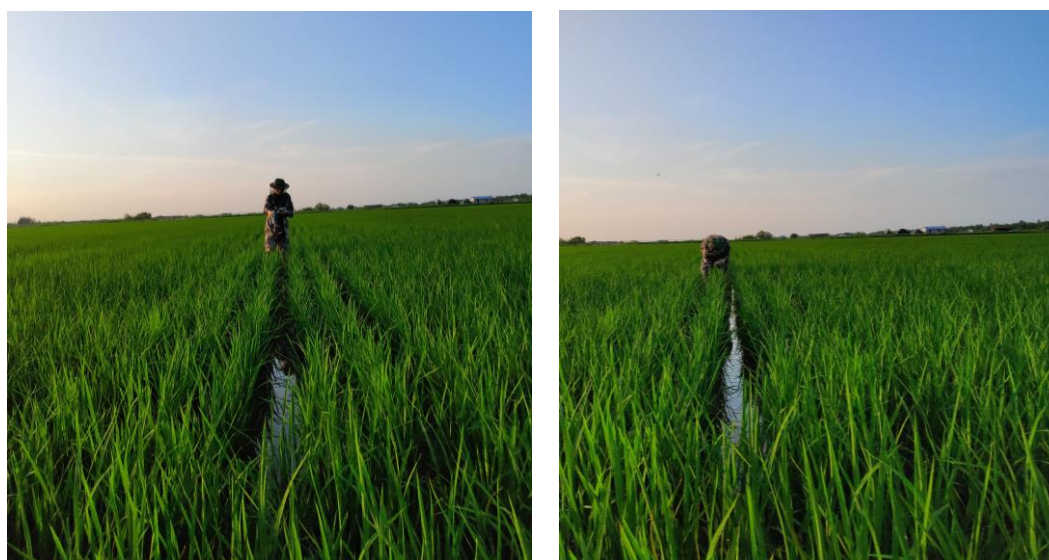


Fig. 4. LAI-2200 field measurement (left: above the canopy; right: below the canopy)

Five concentric conical rings, 7°, 23°, 38°, 53°, 67°, were used to record the incident light under and above the canopy.

The average probability of light penetration into the canopy is computed by

$$\overline{P(\theta_i)} = \frac{1}{N_{obs}} \sum_{j=1}^{N_{obs}} \frac{B_{ij}}{A_{ij}} \quad (1)$$

where the subscript i ($i = 1 \dots 5$) refers to the optical sensor rings centered at θ_i and j refers to the number of observational pairs ($j = 1 \dots N_{obs}$). B_{ij} and A_{ij} are the j^{th} below and above canopy readings, respectively, for the i^{th} ring. The gap fraction for the i^{th} ring is computed from

$$G_i = e^{\overline{(\ln P(\theta_i))}} = e^{\left(\frac{1}{N_{obs}} \sum_{j=1}^{N_{obs}} \ln \frac{B_{ij}}{A_{ij}}\right)} \quad (2)$$

Assuming the foliage elements are randomly distributed in space, the effective PAI (PAI_{eff}) can be estimated by the transmittance in the different view angles based on Miller's formula (Miller, 1967).

$$PAI_{eff} = 2 \int_0^{\pi/2} -\ln P(\theta) \cos \theta \sin \theta d\theta \quad (3)$$

Since multiple observations of $P(\theta)$ are available for LAI-2200, the effective PAI is calculated as

$$PAI_{eff} = 2 \int_0^{\pi/2} -\overline{\ln P(\theta)} \cos \theta \sin \theta d\theta = 2 \sum_{i=1}^5 \overline{K_i} W_i \quad (4)$$

where K_i and W_i are the contact number and the weighting factor, respectively (Table 3).

Table 3. The weighting factors of each ring for LAI-2200.

Ring number	Ring center	Weighting factors
1	7	0.041
2	23	0.131
3	38	0.201
4	53	0.290
5	68	0.337

The weighting factors for the five rings of LAI-2200 are showed in Table 3. LAI-2200 provides the Apparent Clumping Factor ($ACFs$) using the gap fraction measured by five rings (Ryu et al., 2010). $ACFs$ has been considered representing the maximum clumping index for canopy.

$$ACF_s = \frac{2 \int_0^{\pi/2} -\frac{\ln \overline{P(\theta)}}{S(\theta)} \sin \theta d\theta}{2 \int_0^{\pi/2} -\frac{\ln P(\theta)}{S(\theta)} \sin \theta d\theta} = \frac{2 \sum_{i=1}^5 -\frac{\ln \overline{P(\theta_i)}}{S_i} W_i}{2 \sum_{i=1}^5 \overline{K_i} W_i} \quad (5)$$

LAI-2200 calculates the foliage mean tilt angle based on Lang and Xiang (1986), using an empirical polynomial relating inclination angle to the slopes of the idealized curves between 25° and 65° .

The fractional vegetation cover ($fCover$) is calculated by:

$$fCover = 1 - P(7^\circ) \quad (6)$$

where $P(7^\circ)$ is the gap fraction measured on the first ring center at 7° .

3.2 DHP

The DHP images were taken using a Nikon D5100 camera and a 4.5 mm F2.8 EX DC circular fisheye convertor (Fig. 5). An ultraviolet cap was used to prevent dust or rain from the lens. The total height of camera and the lens was about 16.5 cm. Two bubble levels were attached to the camera to keep it horizontal for both downward and upward viewing directions. System calibration for DHP camera was performed before measurement according to the CAN_EYE manual (version 6.4.91), in order to get the optical center and projection function of the lens (Weiss and Baret, 2017).



Fig. 5. Nikon D5100 equipped with Sigma F2.8 EX DC circular fisheye. An ultraviolet cap was used to prevent dust or rain from the lens.

Downward-looking photos were taken. The distance between the camera and the top canopy was set to about 0.8-1.5 m to avoid individual leaves too close to the camera. After that, the aperture and shutter speed of the camera were manually adjusted to avoid over-exposure because the sunlight intensity may change greatly during the measurement direction shifts. To properly sample the spatial variability of the ESU, at least 15 hemispherical photos with a single direction were taken along the sample line (red line in Fig. 1). Nearly all photos were taken under overcast illumination to minimize the shadow effect. All images within an ESU were considered to be under similar illumination conditions. These photos were stored in high-quality JPEG format at a resolution of 3264×4928 .

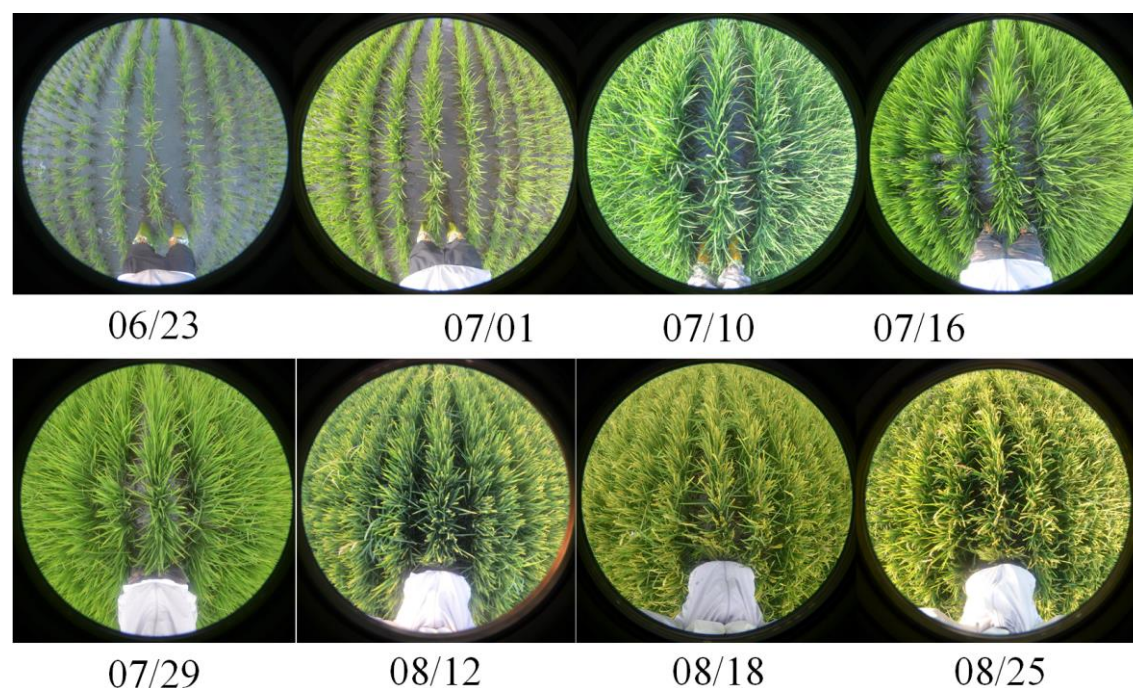


Fig. 6. The downward DHP images obtained during different main growing stages corresponding to Fig. 2: (a) tillering stage (Jun 23 and July 1, 2019); (b) jointing stage (Jul 10 and Jul 16, 2019); (c) flowering stage (Jul 29, and Aug 12, 2019); (d) maturing stage (Aug 18 and Aug 25, 2019).

All valid photos (8~15) over one ESU were processed simultaneously by the CAN_EYE software (version 6.4.91) to extract the structural variables (Weiss et al., 2004). The limit of the image in viewing degrees used in this research (COI) was set to 60° by default. To get a balance between the computation time and images amount, angular resolution for zenith and azimuth directions were set to 10° and the solid angle used in computing the cover fraction was also set to 10° . A threshold process is necessary to separate the foliage from the soil background. To minimize subjective errors, one operator performed all thresholding and classification processes. Fig. 7 presents an example of the downward DHPs classification results in CAN_EYE. More detailed processing procedures can be found in the CAN_EYE manual (version 6.4.91).

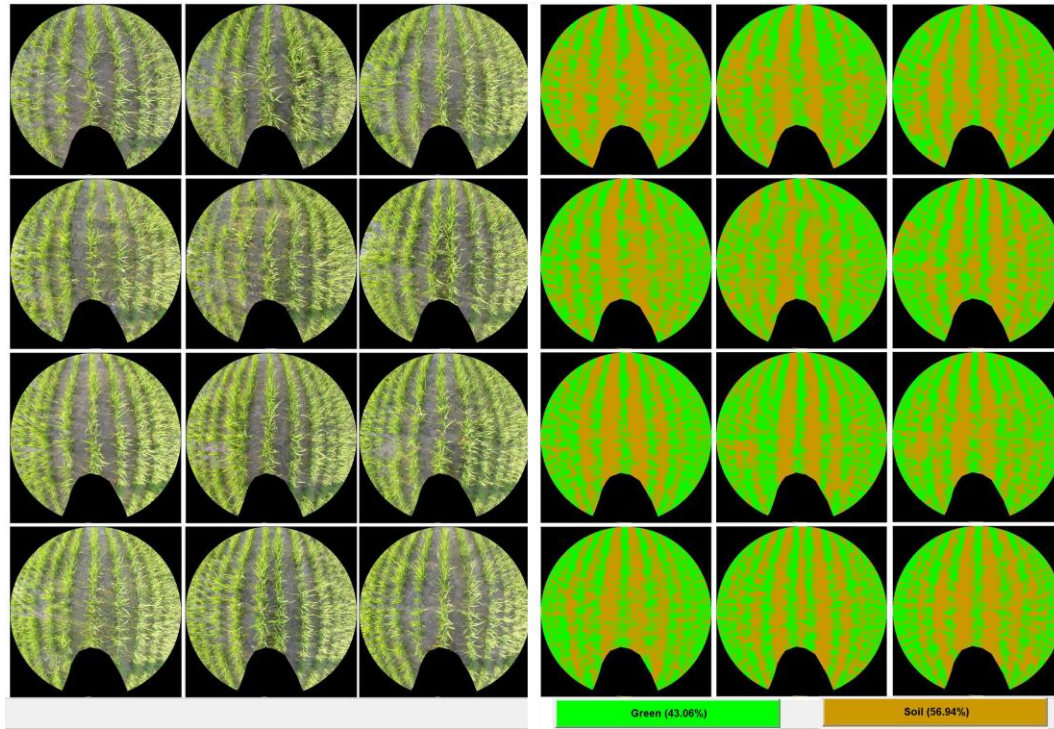


Fig. 7. An example of photo classification in the CAN_EYE software. Green indicates the rice and soil is the background. The operators have been masked.

Assuming an ellipsoidal distribution of the leaf inclination, PAI_{eff} is retrieved using look-up-table techniques with CAN_EYE (Weiss and Baret, 2017). A large range of random combinations of LAI (0 ~ 10) and ALA ($10^\circ \sim 80^\circ$) values are used to build a database following the Beer-Lambert's law (Nilson, 1971) :

$$P(\theta) = e^{-G(\theta) \cdot PAI_{eff} / \cos \theta} \quad (7)$$

where $P(\theta)$ is the canopy gap fraction at the direction θ and $G(\theta)$ is the projection function. By comparing the measured gap fraction and those stored in look-up-table, effective PAI and ALA can be retrieved from Eq. (7) by setting a cost function.

The regularization cost functions used in CAN-EYE V5.1 (Eq. 7 in Weiss and Baret, 2017) and V6.1 (Eq. 8 in Weiss and Baret, 2017) are different. V5.1 tries to constrain the retrieved ALA to be within $60^\circ \pm 30^\circ$, whereas V6.1 tries to minimize the difference between the retrieved PAI and that estimated from the 57° observations. The constraints on V6.1 are efficient without any assumption on ALA; therefore, the V6.1 results are mainly considered for further analysis in this report.

The clumping index (CI) at the direction θ is computed using the logarithm gap fraction averaging method (Lang and Xiang, 1986):

$$CI(\theta) = \frac{\ln \overline{P(\theta)}}{\overline{\ln P(\theta)}} \quad (8)$$

The fraction of vegetation cover ($fCover$) is calculated as the fraction of the soil

covered by the vegetation viewed in the nadir direction.

$$fCover = 1 - P(\theta_{\min}) \quad (9)$$

where $P(\theta_{\min})$ is the gap fraction measured at the smallest view angle θ_{\min} (10°).

3.3 AccuPAR

Decagon's AccuPAR model LP-80 PAR/LAI ceptometer measures photosynthetically active radiation (PAR) using 80 individual sensors (zenith angle is 90°) on its probe (Fig. 10). It measures PAR by locating the probe under and above the canopy and then computes FAPAR based on the four fluxes PAR transmit in the canopy (Widlowski, 2010). Firstly the probe is located above the canopy about 0.8-1.5 m. The probe upward measures the incident PAR (PAR_{in}) and the probe downward measures the PAR reflected by the canopy (PAR_{rc}). Secondly, the probe is located under the canopy about 5 cm above the background soil or shallow water. The probe upward measures the PAR transmitted through the canopy (PAR_{tc}) and the probe downward measures the PAR reflected by the background (PAR_{rs}).

$$FAPAR = \frac{PAR_{in} - PAR_{rc} - PAR_{tc} + PAR_{rs}}{PAR_{in}} \quad (10)$$

The gap fraction (P) is calculated by below

$$P = \frac{PAR_{tc}}{PAR_{in}} \quad (11)$$

Before each measurement, AccuPAR was calibrated according to the instruction manual (when the above canopy PAR is larger than $600 \mu\text{mol}/\text{m}^2\text{s}$). In the field, AccuPAR measurements were taken twice a day at about 10:30 am and 18:00 pm.



Fig. 8. AccuPAR model LP-80 PAR/LAI ceptometer



Fig. 9. AccuPAR field measurement.

3.4 AvaField

Spectral reflectance measurements were acquired with an AvaField-3 portable field spectroradiometer over a spectral range of 300 nm to 2500 nm (Avantes Company, the Netherlands). AvaField 3 has a spectral sampling interval of 0.5 nm between 300 and 1100 nm and 1.0 nm between 1100 and 2500 nm. The radiometer was held by hand and operated in reflect mode with a 22° field of view pointing at the nadir direction. The detector was placed about 1 m above the ground surface. Depending on the atmospheric conditions, a white reference panel was measured every ESU. The readings of the target and the white panel produce reflectance, in which the reflectance of the white panel provided by the manufacturer was also considered. The average reflectance of the sampling points in a plot was used to represent the mean reflectance of that plot.



Fig. 10. AvaField-3 portable field spectroradiometer



Fig. 11. AvaField field measurement

4. Results

Over the season, a total of 574 sets of data at five plots were obtained from the four field measurement methods (Table 4). For each plot, the data were interpolated to obtain a consecutive profile from DOY 173 to DOY 237.

Table 4. Data details at five plots

Structural variables	Field measurement methods	Quantity					Sum
		A	B	C	D	E	
Effective PAI	LAI-2200	9	7	6	7	8	37
	DHP	8	7	7	8	8	38
FAPAR	FAPAR _{am} AccuPAR	7	6	6	6	8	33
	FAPAR _{pm} AccuPAR	8	7	4	6	6	31
	FAPAR _{dir} DHP	8	7	7	8	8	38
	FAPAR _{dif} DHP	8	7	7	8	8	38
	AccuPAR	7	6	6	6	8	33
Gap fraction	LAI-2200	9	7	6	7	8	37
	DHP	8	7	7	8	8	38
Clumping index	LAI-2200	9	7	6	7	8	37
	DHP	8	7	7	8	8	38
ALA	LAI-2200	9	7	6	7	8	37
	DHP	8	7	7	8	8	38
fCover	LAI-2200	9	7	6	7	8	37
	DHP	8	7	7	8	8	38
Spectral reflectance curve	AvaField	5	5	5	5	6	26

4.1 Effective PAI

The effective PAI estimated from LAI-2200 and the downward DHP is shown in Fig. 12. The five plots follow fairly consistent seasonal phenological stages of LAI changes. LAI increases after transplant until end of July (DOY=210), reaches a maximum at around 5, and then begins to decrease at late August (DOY=230). The results show that the measurement results of the two instruments are basically consistent. The discrepancies between the optical instruments increase and then decrease during the season reach the largest discrepancies in early August.

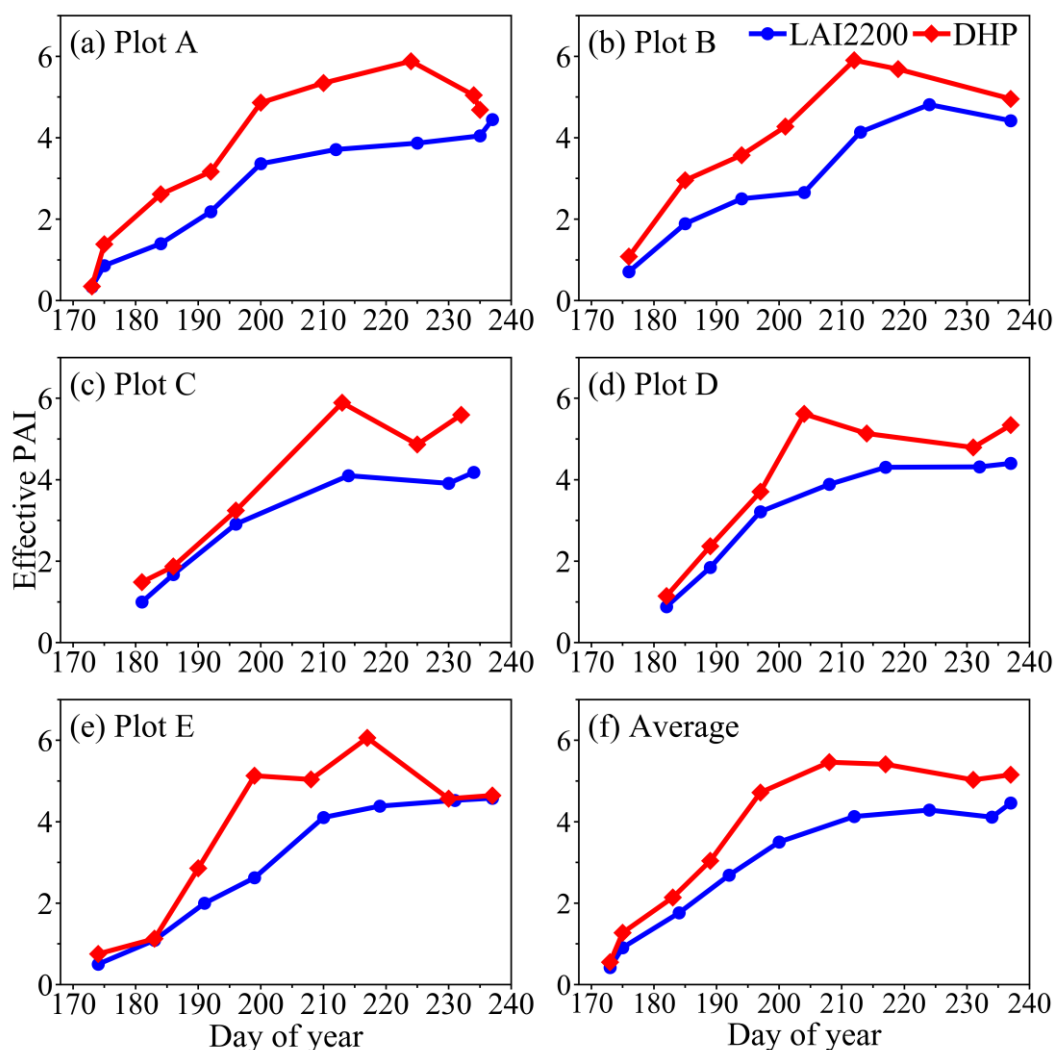


Fig. 12. Seasonal variation of the effective PAI (PAI_{eff}) estimated from LAI-2200, DHP, for the five plots. Panels (a)–(e) for plots A–E and panel (f) the average of all plots.

4.2 FAPAR

The FAPAR estimated from the AccuPAR and the DHP is shown in Fig. 13. The five plots follow fairly consistent seasonal phenological stages of FAPAR changes. FAPAR increases after transplant until end of July (DOY=200), reaches a maximum at around 0.9. The FAPAR_{dir} and FAPAR_{dif} estimated from DHP keep consistent at different plots over the season. The FAPAR estimated from DHP is slightly larger than the FAPAR estimated from the AccuPAR due to the different defines of FAPAR. The FAPAR_{pm} is larger than the FAPAR_{am} overall. A few FAPAR_{pm} anomalies existed because the measurement time is earlier than 17:00 pm.

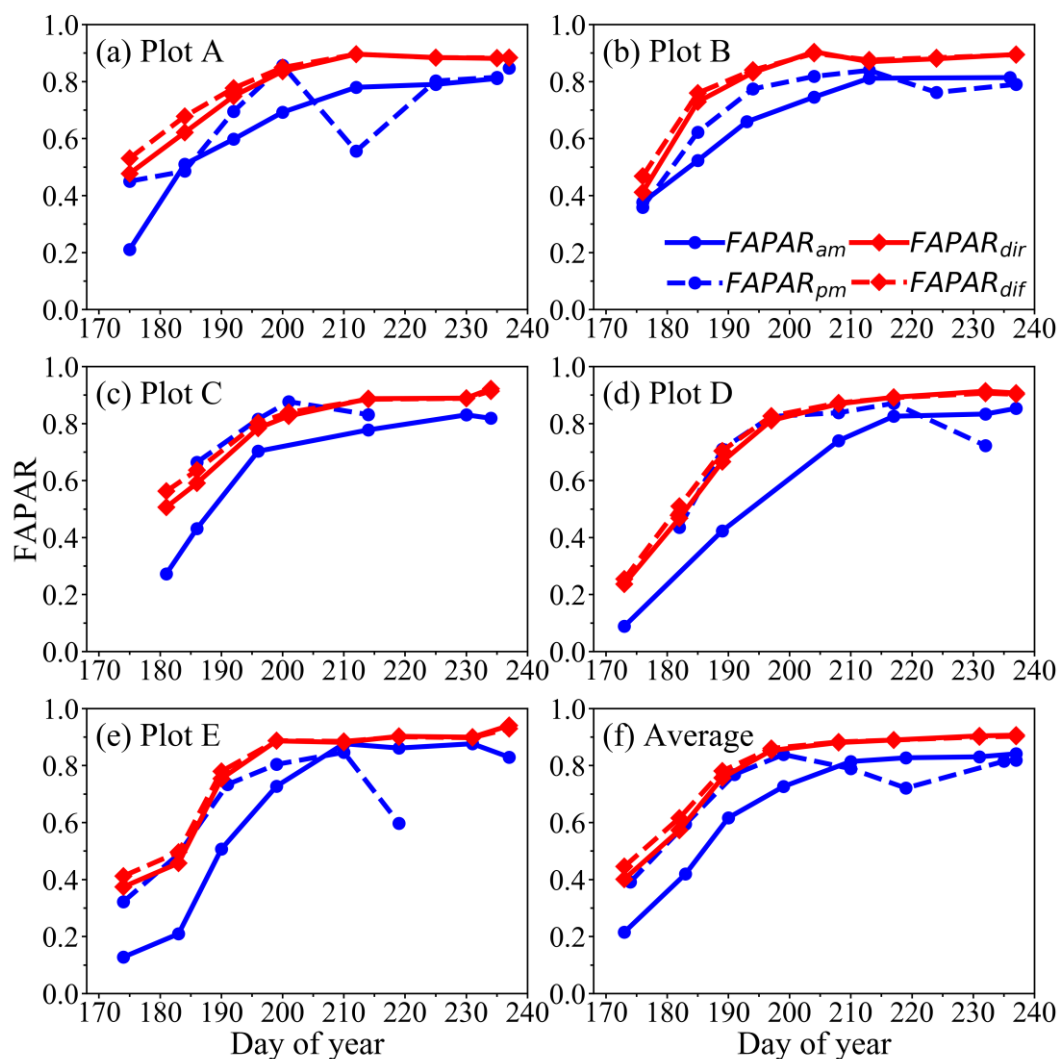


Fig. 13. Seasonal variations of the FAPAR in the morning (10:30 am, $FAPAR_{am}$) and afternoon (18:00 pm, $FAPAR_{pm}$) estimated from AccuPAR and diffuse FAPAR ($FAPAR_{dif}$), direct FAPAR ($FAPAR_{dir}$) from DHP for the five plots. Panels (a)–(e) for plots A–E and panel (f) the average of all plots.

4.3 Gap fraction

The angular gap fractions estimated from LAI-2200 and DHP are shown in Fig. 14. The optically obtained gap fractions generally decline with the development of canopy leaves and remain unchanged after DOY=210. The gap fraction generally decreases with the increase of view zenith angle in the whole season. On average, the gap fraction for the DHP is similar to that of the AccuPAR and is slightly larger than that of the LAI-2200.

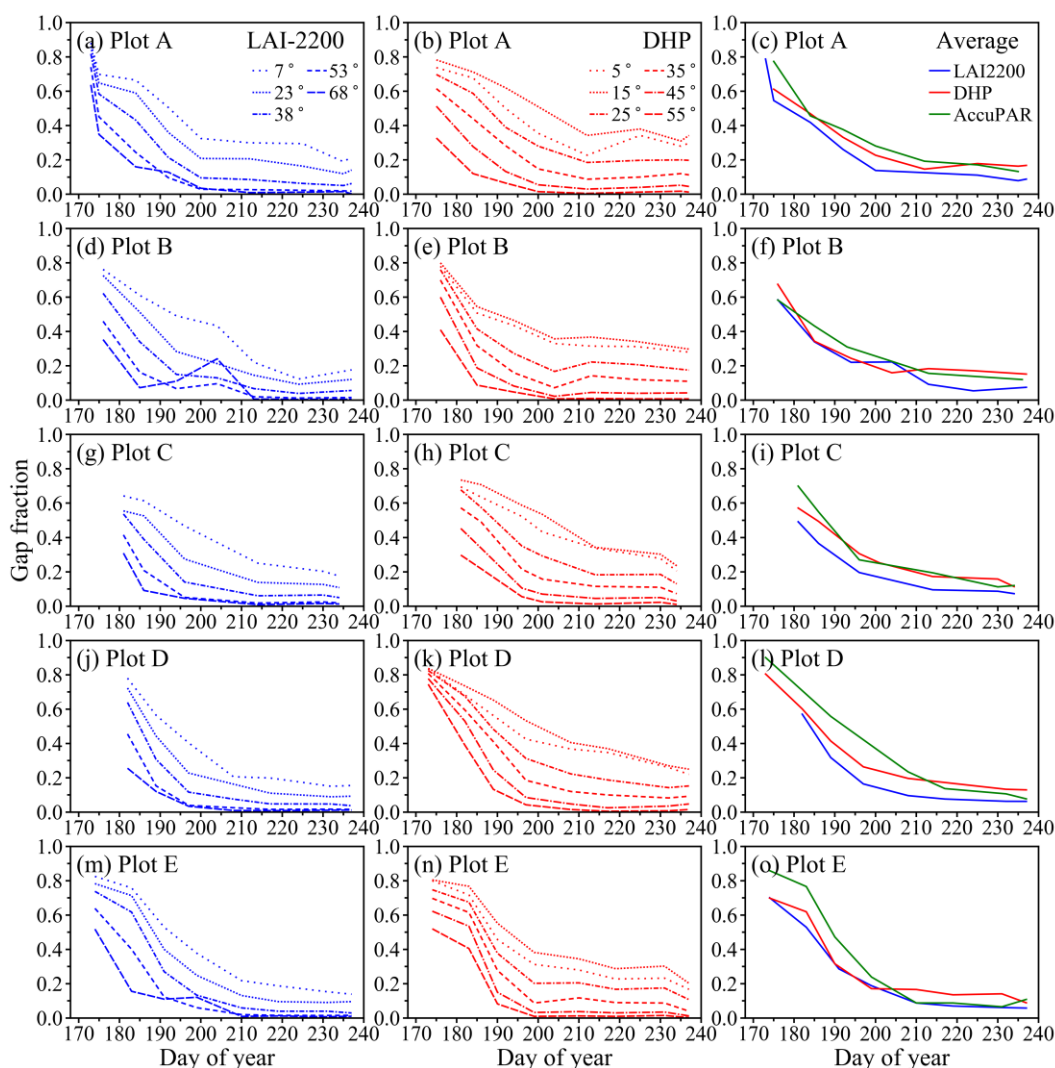


Fig. 14. Seasonal variations of the gap fraction at different view zenith angles from LAI-2200 and DHP. For DHP, the measured effective gap fractions from CAN_EYE V6.1 are shown. The Panel of the last column shows the average gap fractions from LAI-2200 and DHP and the transmittance from AccuPAR at about 10:30 am.

4.4 Clumping index

Fig. 15 presents the seasonal dynamics of CI estimated from the DHP and the ACF from LAI-2200. CI decreases after transplant until mid-July (DOY=190). CI generally increases with the increase of view zenith angle before mid-July (DOY=190) but decreases after mid-August (DOY=220). In contrast, ACF from LAI-2200 shows little seasonal variation for all angles. ACF generally decreases with the increase of view zenith angle in the whole season. The average ACF is systematically higher than the CI values estimated from the DHP.

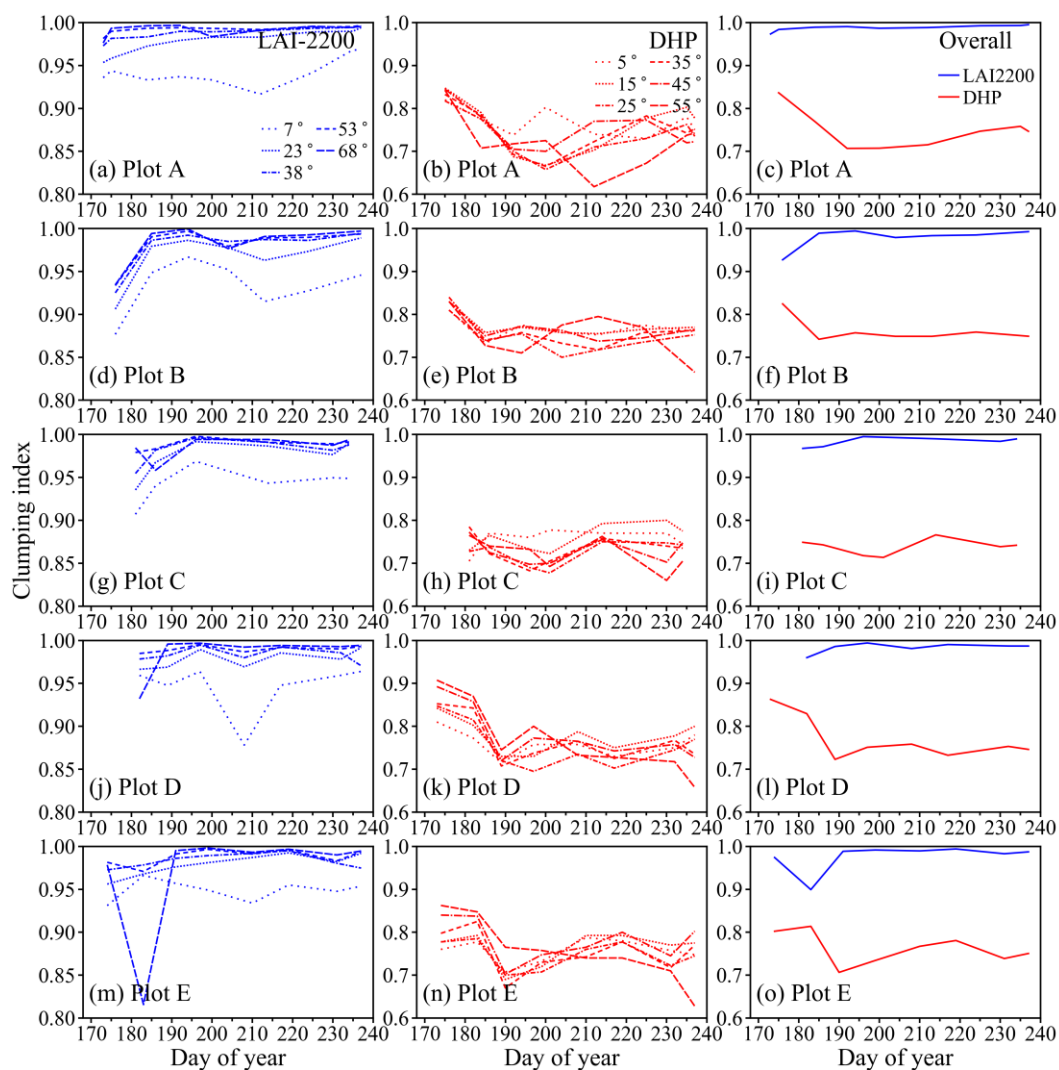


Fig. 15. Seasonal variation of the clumping indices (CI) at different view zenith angles from LAI-2200 and DHP. The Panel of the last column shows the overall CI from LAI-2200 and DHP.

4.5 fCover

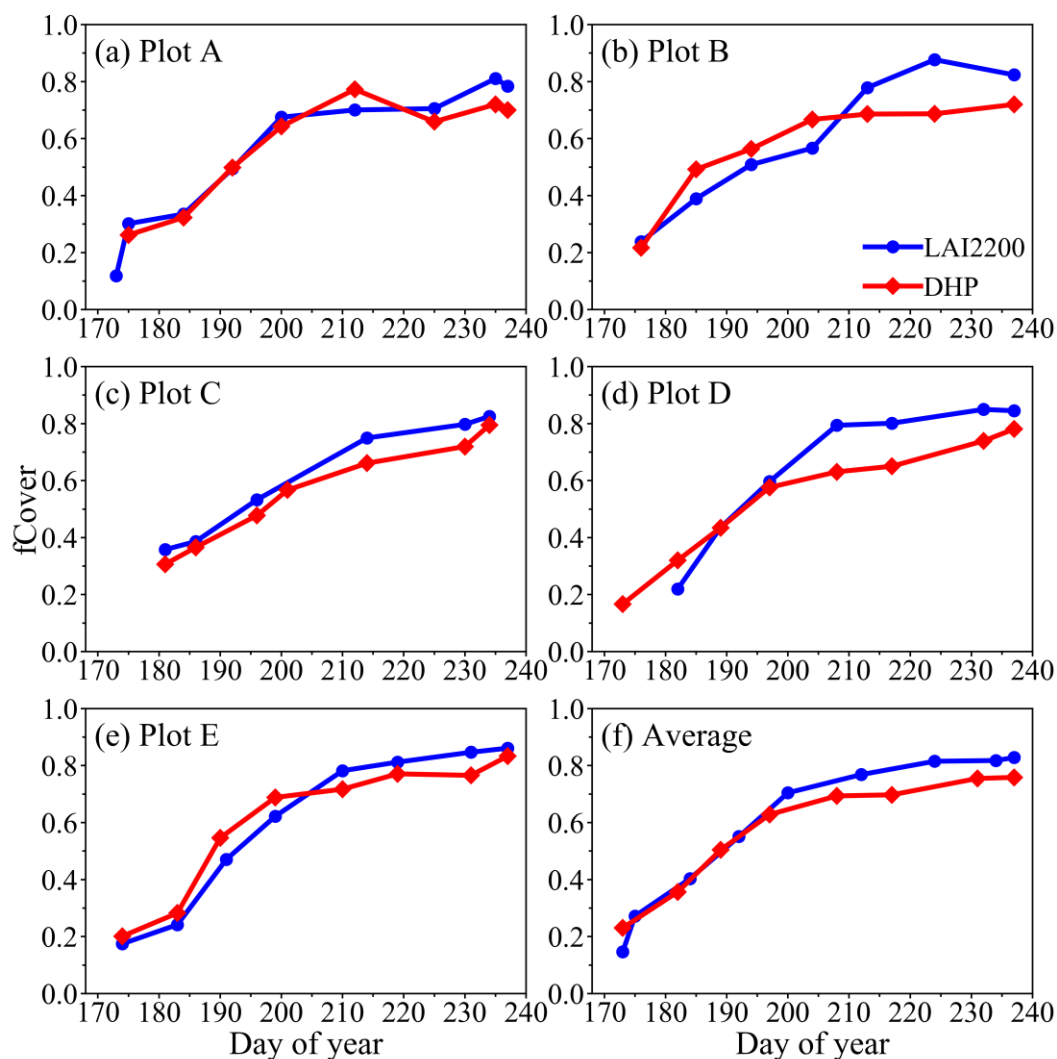


Fig. 16. Seasonal variations of fCover calculated from LAI-2200 and DHP

The seasonal variation of fCover estimated from LAI-2200 and DHP is shown in Fig. 16. The fCover estimated from the two optical instruments increases with the season, reaching a maximum value of ~ 0.8 . The results show that the measurement results of the two instruments are basically consistent. Note that the fCover is calculated from the gap fraction, and it represents the whole coverage including green leaves, yellow leaves, stems and seeds.

4.6 ALA

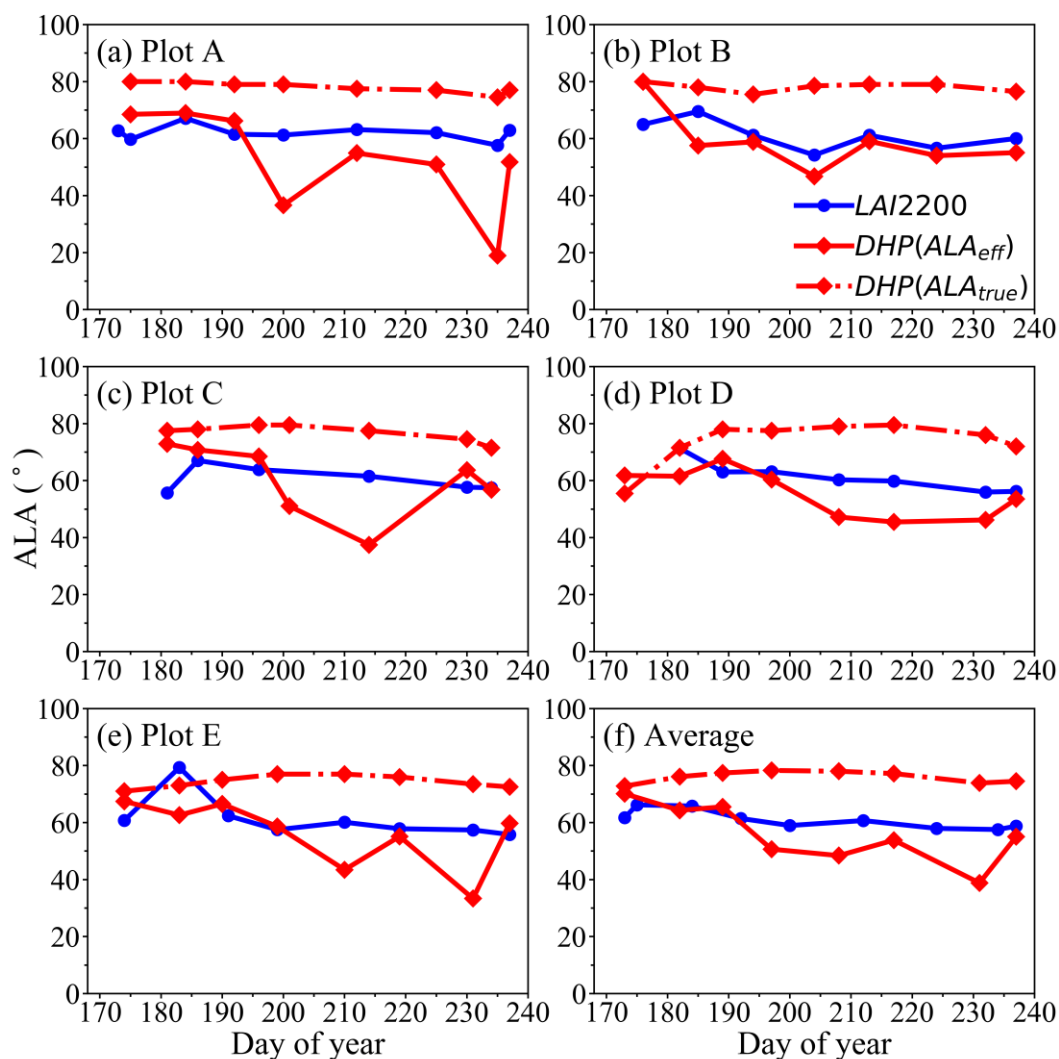


Fig. 17. Seasonal variation of ALA calculated from LAI-2200 and DHP. Solid and dashed lines represent effective and true ALAs retrieved from DHP, respectively.

The seasonal dynamics of ALAs estimated from LAI-2200, DHP are presented in Fig. 17. ALA from LAI-2200 and the true ALA retrieved from the DHP show little seasonal variation. In contrast, the effective ALA from the DHPs shows strong variations. The true ALAs are systematically higher than the effective ALAs.

4.7 Spectral reflectance curve

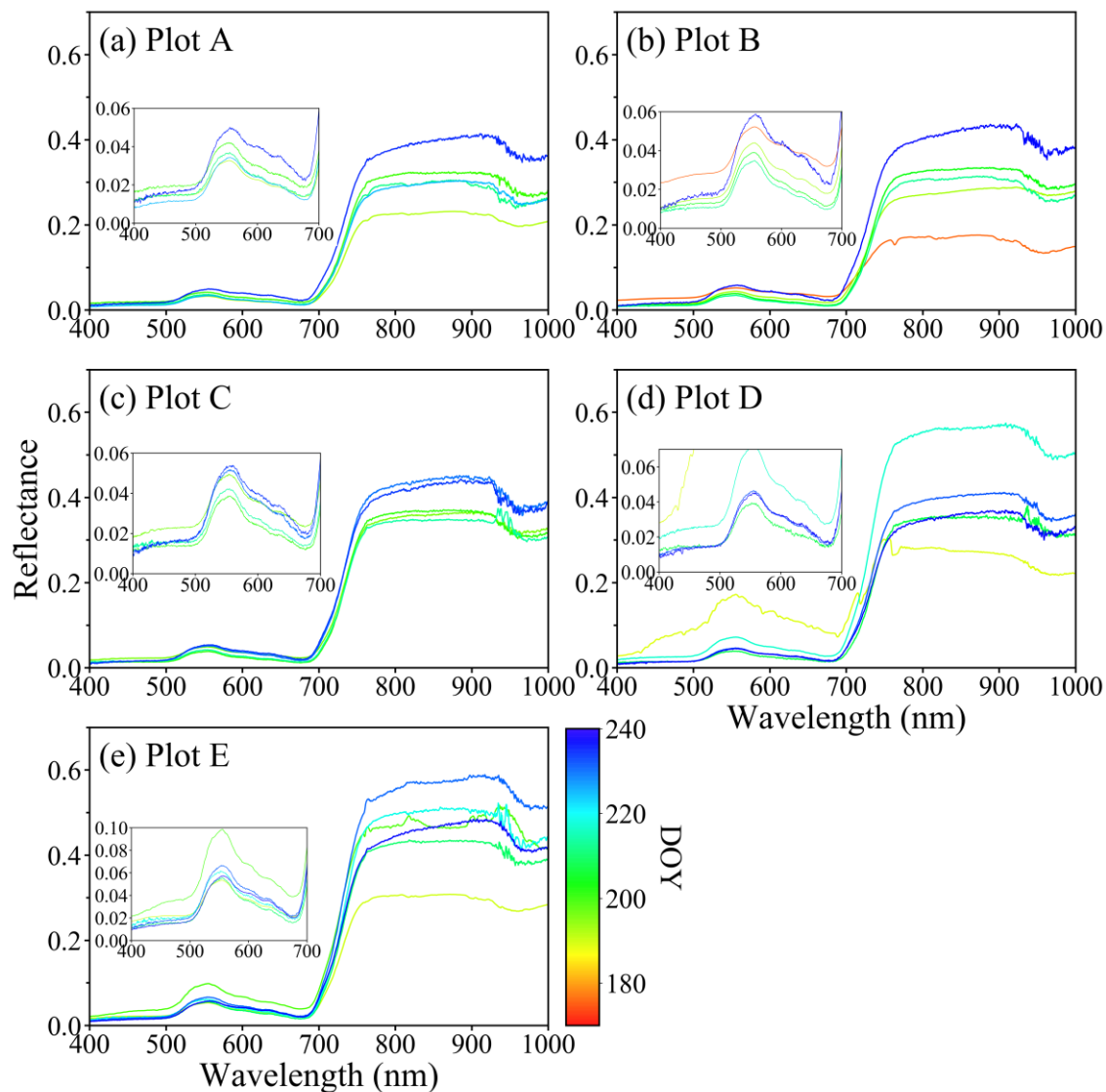


Fig. 18. Spectral reflectance curve (400 nm–1000 nm) measured over the season.

Fig. 18 shows the spectral reflectance curve with the wavelength from 400 nm to 1000 nm over the season. The canopy reflectance showed clear seasonal variations. The spectrum showed a green reflectance peak at 400–700 nm (VIS) and a platform at 750–950 nm (NIR). The reflectance at the NIR band before mid-July (DOY=190) is much lower than that after end-July (DOY=200) because of the water features (Sun et al., 2017).

5. Quality assurance

The study area is considered homogeneous at a $3 \times 3 \text{ km}^2$ area. The five plots are located away from the road, irrigation canals and ditches. The field management practices and environmental conditions are similar to these plots. Weekly field measurement began right after the transplantation and ended when the rice was maturing. LAI2200, DHP and FAPAR were performed under diffuse radiation conditions, i.e., near the sunset at about 18:00 pm or during overcast days. And the FAPAR and AvaField were also performed at about 10:30 am under the sunny day.

The optical instruments were used before in the field campaign (Fang et al., 2018, 2014; Jiang and Fang, 2019; Sun et al., 2017). Instrument calibrations were performed before or during the measurements, according to the instrument manual.

6. Data access and citation

6.1 Data access

All final results over each plot are provided, including PAI, PAI_{eff}, FAPAR, gap fraction, CI, ALA and fCover. They are compiled in ASCII format. Please contact the PI below for the field measured and the processed data.

Prof. Hongliang Fang

LREIS, Institute of Geographic Sciences and Natural Resources Research

Chinese Academy of Sciences (CAS)

11A Datun Road, Room 1318

Beijing, 100101, China

Tel: (8610) 64888055

Fax: (8610) 64889630

Email: fanghl@lreis.ac.cn

6.2 Citation

Hongliang Fang, Yinghui Zhang, Yao Wang, Sijia Li, 2020. Paddy Rice Experiment in the Sanjiang Plain (PRESP 2019): Field Measurement Report. Institute of Geographic Sciences and Natural Resources Research, Chinese Academy of Sciences. <http://www.lreis.ac.cn/kfjl/zlxz/>

References

- Fang, H., Li, W., Wei, S., Jiang, C., 2014. Seasonal variation of leaf area index (LAI) over paddy rice fields in NE China: Intercomparison of destructive sampling, LAI-2200, digital hemispherical photography (DHP), and AccuPAR methods. *Agricultural and Forest Meteorology* 198, 126–141.
- Fang, H., Ye, Y., Liu, W., Wei, S., Ma, L., 2018. Continuous estimation of canopy leaf area index (LAI) and clumping index over broadleaf crop fields: An investigation of the PASTIS-57 instrument and smartphone applications. *Agricultural and Forest Meteorology* 253–254, 48–61. <https://doi.org/10.1016/j.agrformet.2018.02.003>
- Jiang, C., Fang, H., 2019. GSV: a general model for hyperspectral soil reflectance simulation. *International Journal of Applied Earth Observation and Geoinformation* 83, 101932. <https://doi.org/10.1016/j.jag.2019.101932>
- Lang, A.R.G., Xiang, Y., 1986. Estimation of leaf area index from transmission of direct sunlight in discontinuous canopies. *Agricultural and Forest Meteorology* 37, 229–243. [https://doi.org/10.1016/0168-1923\(86\)90033-X](https://doi.org/10.1016/0168-1923(86)90033-X)
- Nilson, T., 1971. A theoretical analysis of the frequency of gaps in plant stands. *Agricultural Meteorology* 8, 25–38. [https://doi.org/10.1016/0002-1571\(71\)90092-6](https://doi.org/10.1016/0002-1571(71)90092-6)
- Ryu, Y., Nilson, T., Kobayashi, H., Sonnentag, O., Law, B.E., Baldocchi, D.D., 2010. On the correct estimation of effective leaf area index: Does it reveal information on clumping effects? *Agricultural & Forest Meteorology* 150, 463–472.
- Song, C., Xu, X., Tian, H., Wang, Y., 2009. Ecosystem-atmosphere exchange of CH₄ and N₂O and ecosystem respiration in wetlands in the Sanjiang Plain, Northeastern China. *Global Change Biology* 15, 692–705. <https://doi.org/10.1111/j.1365-2486.2008.01821.x>
- Sun, T., Fang, H., Liu, W., Ye, Y., 2017. Impact of water background on canopy reflectance anisotropy of a paddy rice field from multi-angle measurements. *Agricultural and Forest Meteorology* 233, 143–152.
- Weiss, M., Baret, F., 2017. *Can_Eye V6.4.91 User Manual* 56.
- Weiss, M., Baret, F., Smith, G.J., Jonckheere, I., Coppin, P., 2004. Review of methods for in situ leaf area index (LAI) determination: Part II. Estimation of LAI, errors and sampling. *Agricultural and Forest Meteorology* 121, 37–53.
- Widlowski, J.L., 2010. On the bias of instantaneous FAPAR estimates in open-canopy forests. *Agricultural and Forest Meteorology* 150, 1501–1522. <https://doi.org/10.1016/j.agrformet.2010.07.011>
- Yang, W., Hao, F., Cheng, H., Lin, C., Ouyang, W., 2013. Phosphorus fractions and availability in an albic bleached meadow soil. *Agronomy Journal* 105, 1451–1457. <https://doi.org/10.2134/agronj2013.0204>

Table 5. Field measurement log

Date	DOY	Weather	Plot	AM/PM	Field measurement methods	Time (HHMM-HHMM)	Notes
2019/6/22	173	Sunny, Few clouds	PlotD	AM	AccuPAR	1000-1100	3 ESUs are measured.
					AccuPAR	0700-0730	
				PM	LAI2200	0630-0700	
	DHP	0630-0700					
2019/6/23	174	Sunny	PlotE	AM	AccuPAR	1000-1030	
					AccuPAR	0630-0700	
				PM	LAI2200	0630-0700	
		DHP	0630-0730				
2019/6/24	175	Sunny, cloud	PlotA	AM	AccuPAR	1000-1030	
					AccuPAR	0630-0700	
				PM	LAI2200	0630-0730	
		DHP	0630-0730				
2019/6/25	176	Overcast	PlotB	AM	AccuPAR	1000-1030	
					AvaField	0930-1000	
					AccuPAR	0600-0630	
		PM	LAI2200	0630-0700			
		DHP	0630-0730				
2019/6/30	181	Overcast to drizzle	PlotC	AM	AccuPAR	0930-1000	Because of rains, the depth of water background is more than 10cm
					LAI2200	0900-0930	
					DHP	0900-0930	
2019/7/1	182	Overcast	PlotD	PM	AccuPAR	0500-0530	Rice height: 50cm, water depth: 12cm

					LAI2200	0500-0530	
					DHP	0500-0530	
				AM	AccuPAR	0930-1000	
2019/7/2	183	Overcast	PlotE		AccuPAR	0445-0530	
				PM	LAI2200	0500-0530	
					DHP	0500-0530	
					AccuPAR	0930-1000	
2019/7/3	184	Overcast	PlotA	AM	LAI2200	0930-1000	Spots appear on the leaves and a layer of green algae floats on the water background
					DHP	0930-1000	
				PM	AccuPAR	0445-0530	
					AccuPAR	1000-1030	
2019/7/4	185	Overcast to Sunny	PlotB	AM	DHP	1000-1030	The water is emptied in the paddy fields for medicine.
				PM	AccuPAR	0500-0530	
					LAI2200	0500-0530	
				AM	AccuPAR	1000-1030	
2019/7/5	186	Overcast to Sunny	PlotC		DHP	1000-1030	
				PM	AccuPAR	0500-0530	
					LAI2200	0500-0530	
				AM	AccuPAR	1000-1030	
2019/7/8	188	Sunny, Few clouds	PlotD		AvaField	0930-1000	
					AccuPAR	0500-0530	
				PM	LAI2200	0530-0600	
					DHP	0500-0531	
					AccuPAR	1000-1030	
2019/7/9	189	Sunny, cloud	PlotE	AM	AvaField	0930-1000	
2019/7/10	190	Sunny		PM	AccuPAR	0500-0530	

					LAI2200	0530-0600	
					DHP	0500-0531	
				AM	AccuPAR	1000-1030	
					AvaField	0930-1000	
2019/7/11	191	Sunny,cloud	PlotA		AccuPAR	0500-0530	
				PM	LAI2200	0530-0600	
					DHP	0500-0531	
2019/7/12	192	Sunny to drizzle	PlotB	AM	AccuPAR	1000-1030	
					AvaField	0930-1000	
					AccuPAR	0500-0530	The water is emptied in the paddy fields for medicine.
2019/7/13	193	Sunny,cloud	PlotB	PM	LAI2200	0500-0530	
					DHP	0500-0531	
				AM	AccuPAR	0930-1000	
					AvaField	0930-1000	
2019/7/15	195	Sunny,cloud	PlotC		AccuPAR	0500-0530	
				PM	LAI2200	0500-0531	
					DHP	0500-0531	
					AccuPAR	0500-0530	
2019/7/16	196	Sunny,cloud	PlotD	PM	LAI2200	0500-0531	
					DHP	0500-0531	
				AM	AccuPAR	1030-1100	
					AvaField	0930-1030	
2019/7/18	198	Sunny,cloud	PlotE		AccuPAR	0500-0530	Rice starts to spike
				PM	LAI2200	0500-0531	
					DHP	0500-0531	
2019/7/19	199	Overcast to	PlotA	AM	AccuPAR	1030-1100	Rice starts to spike

		Sunny		AvaField	0930-1030	
				AccuPAR	0500-0530	
			PM	LAI2200	0500-0531	
				DHP	0500-0531	
			AM	AvaField	1100-1130	
2019/7/20	200	Sunny,Few clouds	PlotC	AccuPAR	1600-1630	
			PM	DHP	1600-1630	
				AccuPAR	1030-1100	
			AM	AvaField	0930-1030	
2019/7/23	203	Sunny,cloud	PlotB	AccuPAR	0500-0530	Overgrown weeds in the plot, especially ESU4 / 2. Weeds in the two ESUs were different. ESU2 contains aquatic weeds, and ESU4 contains upland weeds, which are similar to rice.
			PM	LAI2200	0500-0530	
				DHP	0500-0530	
			AM	AccuPAR	1000-1030	
				AvaField	1000-1030	
2019/7/27	207	Sunny,cloud	PlotD	AccuPAR	1600-1630	Rice starts to spike
			PM	LAI2200	1600-1630	
				DHP	1600-1630	
			AM	AccuPAR	0930-1000	
				AvaField	0930-1001	Rice in ESU2 and ESU3 starts to spike
2019/7/29	209	Sunny,cloud	PlotE	AccuPAR	1700-1730	
			PM	LAI2200	1700-1730	
				DHP	1700-1731	
			AM	AccuPAR	0930-1029	
2019/7/31	211	Sunny,cloud	PlotA	AvaField	0930-1030	Some rice spikes turn grayish red
			PM	AccuPAR	0500-0530	

2019/8/1	212	Sunny,Few clouds	PlotB	AM	LAI2200	0500-0531	Weeds in the field
					DHP	0500-0531	
					AccuPAR	0930-1029	
				PM	AvaField	0930-1030	
					AccuPAR	0500-0530	
					LAI2200	0500-0531	
2019/8/2	213	Sunny,Few clouds	PlotC	AM	DHP	0500-0531	
					AccuPAR	1000-1030	
					AvaField	1000-1030	
				PM	AccuPAR	1700-1730	
					LAI2200	1700-1730	
					DHP	1700-1731	
2019/8/5	217	Sunny,Few clouds	PlotD	AM	AccuPAR	0930-1029	
					AvaField	0930-1030	
					AccuPAR	0500-0530	
				PM	LAI2200	0500-0531	
					DHP	0500-0531	
					AccuPAR	1030-1100	
2019/8/7	219	Overcast	PlotE	AM	AvaField	1030-1100	
					AccuPAR	1630-1700	
					LAI2200	1630-1700	
				PM	DHP	1630-1700	
					AccuPAR	1730-1800	
					LAI2200	1730-1800	
2019/8/12	224	Sunny	PlotB	PM	DHP	1730-1800	
					AccuPAR	1730-1800	
					LAI2200	1730-1800	

2019/8/13	225	Sunny	PlotA	AM	AccuPAR	1000-1030	
					AvaField	1000-1031	
				PM	AccuPAR	1700-1729	
					LAI2200	1700-1730	
2019/8/18	230	Cloudy	PlotC	AM	DHP	1700-1731	
					AccuPAR	0930-1029	
					AvaField	0930-1030	
					LAI2200	0930-1031	
2019/8/19	231	Cloudy	PlotE	AM	DHP	0930-1032	
					AccuPAR	0930-1029	
					AvaField	0930-1030	
					LAI2200	0930-1031	
2019/8/20	232	Sunny,Few clouds	PlotD	AM	AccuPAR	1000-1030	
					AvaField	1000-1030	
				PM	AccuPAR	1630-1700	
					LAI2200	1630-1700	
2019/8/22	234	Overcast drizzle	to PlotC	AM	DHP	1630-1700	
					AccuPAR	0930-1029	
					AvaField	0930-1030	
					LAI2200	0930-1031	
2019/8/23	235	Overcast drizzle	to PlotA	AM	DHP	0930-1032	
					AccuPAR	0930-1029	
					AvaField	0930-1030	
					LAI2200	0930-1031	
					DHP	0930-1032	

It rained in the early morning, and there are rains on the rice leaves.

2019/8/24	236	Overcast	PlotB	AM	AccuPAR	0930-1029		
					AccuPAR	1730-1800		
			PlotB	PM	LAI2200	1730-1801		
					DHP	1730-1802		
					AccuPAR	0900-0930		
					AvaField	0900-0931		
			PlotD	AM	LAI2200	0900-0932		
					DHP	0900-0933		
					AccuPAR	1000-1030		
					AvaField	1000-1031		
LAI2200	1000-1032							
DHP	1000-1033							
2019/8/25	237	Sunny,cloud	PlotE	AM	AccuPAR	1600-1630		
					AvaField	1600-1631		
					LAI2200	1600-1632		
					DHP	1600-1633		
					PlotA	PM	AvaField	1600-1631
					LAI2200		1600-1632	
			DHP	1600-1633				
